Template-free and spontaneous formation of vertically aligned Pd nanofiber arrays at the liquid-liquid interface between redox-active ionic liquid and water

Yu Zhang,[a] Naoya Nishi[a] and Tetsuo Sakka[a]*

[a] Y. Zhang, N. Nishi, T. Sakka

Department of Energy and Hydrocarbon Chemistry, Graduate School of Engineering, Kyoto University.

Kyoto 615-8510, Japan.

E-mail: nishi.naoya.7e@kyoto-u.ac.jp

Abstract

Vertically aligned Pd nanofiber arrays (NFAs) have been prepared at the liquid-liquid interface between redox-active ionic liquid (RAIL) and water (W) via a template-free manner. The RAIL with high hydrophobicity, (ferrocenylmethyl)dodecyldimethylammonium bis(nonafluorobutanesulfonyl) amide, plays dual roles of reducing agent for Pd precursor ions and the hydrophobic liquid phase simultaneously, and the RAIL|W interface has been utilized as the formation site for the spontaneous growth of Pd NFAs. The Pd NFAs consist of three parts: layers formed by partly connected particles on the top, NFAs in the middle, and firm sheet-like layers on the bottom. Owing to the top and bottom supporting layers, the anti-deformation ability and durability of the Pd NFAs with a length reaching several micrometers are enhanced. A possible mechanism for the formation of the Pd NFAs has been discussed. The Pd NFAs show a good stability and a higher electrocatalytic activity toward ethanol oxidation reaction than a commercial Pd/C catalyst. The present study provides a new strategy for the template-free and spontaneous formation of Pd NFAs.

KEYWORDS: Ionic liquid|water interface; electron transfer; ion transfer; ITIES; electrodeposition.

INTRODUCTION

Metal nanostructures have drawn considerable interest in various research

areas by virtue of the optical, electrical, and catalytic properties that bulk metals do not exhibit. [1-3] However, due to the high surface energy of structures with nanoscale, aggregation of nanostructures has been regarded as a great barrier, since the application performance could be severely hindered by the loss of the surface area. A frequently adopted strategy for preventing the nanostructures from aggregation is the use of capping agents.[4, 5] Nevertheless, it was reported that some capping agents may act as "surface poisons",[6] lowering the catalytic activities of nanostructures by blocking active sites.

The architectural way of thinking can be incorporated into nanostructure designs, and provides nanostructures with particular architectural advantages such as anti-aggregation and anti-deformation abilities. Architectural nanostructures[7-9] are built up by the orderly combination or arrangement of simple nano units. One kind of architectural nanostructures is one dimensional (1D) nanoarrays, which are a series of orderly aligned 1D nano units standing on substrates, including nanobelt,[10, 11] nanowire,[12-14] nanofiber,[15] and nanotube[16] arrays. They have shown promising application potential in nanodevice[17] and catalysis.[18] Such kind of orderly aligned 1D structures on substrates can resist aggregation to a great extent, since the 1D units are spatially fixed on substrates, and therefore are inhibited from moving freely to get in contact with each other. However, there still lacks a facile method for the preparation of 1D nanoarrays. By far, an extensively recognized method is to use porous anodic aluminum oxide (AAO) as a template to confine

the growth of nanoarrays.[19-23] However, this method requires the formation and removal procedures of the AAO template, increasing the difficulties and spending time and energy during the synthesis process. Additionally, the length of 1D nanoarrays is commonly limited by the thickness of the AAO template. Moreover, when the length-to-diameter ratio of 1D nanoarrays is large, the lack of bearing points from the top could induce the deformation from the architectural perspective.

The oil (O)|water (W) interface is an inhomogeneous region having a thickness on the order of a few angstroms.[24] It has been applied as the formation site for the preparation of Au nanostructures over the last few decades.[25-29] The deposition of Au is spatially restricted at the O|W interface, by using metal precursor only soluble in one phase and reducing agent only soluble in the other phase. In recent years, the liquid-liquid (L|L) interfacial method has been extensively developed for the deposition of several noble metals such as Pt,[30,31] Ag,[32-34] Cu[35, 36] and Pd.[37-39] Pd is remarkably famed for the excellent performance in hydrogen storage, gas sensing, and especially catalysis. Johans *et al.* presented a model for diffusion controlled electrodeposition of Pd particles at the O|W interface, and the nucleation at the O|W interface has been studied by means of the electrochemical measurements.[40,41] Lahtinen *et al.* prepared Pd particles by a heterogeneous redox reaction at the O|W interface, and then applied the interfacial Pd nanoparticles as reductive photocatalysts for a photo-induced two-phase redox reaction.[42] Dryfe *et al.* prepared Pd nanoparticles at the O|W interface by externally

controlling the phase boundary potential across the O|W interface.[37, 43-46]

Recently, growing interest has been drawn on replacing organic solvents by hydrophobic ionic liquids (ILs) in the L|L interfacial method.[47-50] ILs are liquid salts which are entirely composed of cations and anions. Hence, the properties of ILs can be controlled by elaborate designs of the chemical structures of constituting ions, endowing ILs with active functions in the IL|W system. For instance, the morphology of Ag nanostructures formed at the IL|W interface can be affected by using ILs with different ions.[51] Chen *et al.* fabricated Pd nanostructures at the IL|W interface, and the IL ions were found to be selectively adsorbed on the metal surface and to play a role of the template.[52] In our previous studies, the L|L interfacial method by using the electrochemically polarizable IL|W interface was proved to be a valid strategy for the preparation of noble metal nanofibers.[53-55]

Due to their designability, ILs can play multiple roles rather than just as a solvent. When ILs contain redox-active groups in the cation or anion, the IL itself can be the reducing agent for the metal precursor ions and the hydrophobic liquid phase in the L|L interfacial method simultaneously. Samec *et al.* prepared a redox-active IL (RAIL), (ferrocenylmethyl)dodecyldimethylammonium tetrakis[3,5-bis(trifluoromethyl)phenyl]borate ([$FcMDDA^+$][$TFPB^-$]), to form the electrochemically polarizable RAIL|W interface, and succeeded in measuring the electron transfer (ET) across the RAIL|W interface between $FcMDDA^+$

constituting the RAIL and redox species dissolved in W.[56, 57] However, up till now, there is no precedent report on the use of RAIL to prepare metal nanostructures at the RAIL|W interface.

In the present paper, we present a template-free strategy for preparing vertically aligned Pd nanofiber arrays (NFAs) with supporting Pd layers at the top and bottom, both of which provide high stability for the NFAs with height even up to several micrometers. A hydrophobic RAIL, (ferrocenylmethyl)dodecyldimethylammonium bis(nonafluorobutanesulfonyl)amide ($[FcMDDA^+][C_4C_4N^-]$), was prepared and employed as the reducing agent as well as the hydrophobic liquid phase to form the electrochemically polarizable RAIL|W interface, which was adopted as the formation site for the spontaneous growth of the Pd NFAs. The reaction time and concentration dependence experiments reveal that the neat and vertical arrangement of the Pd NFAs highly relies on the top and bottom supporting Pd layers. The long term stability check manifests that the Pd NFAs can resist aggregation and deformation in a liquid environment for over seven months. A possible mechanism for the spontaneous formation of the Pd NFAs is discussed. The Pd NFAs show a good stability and a higher electrocatalytic activity toward ethanol oxidation reaction than a commercial Pd/C catalyst. The present study proposes a new concept for designing and preparing architectural nanostructures by using the soft L|L interface as the reaction site.

RESULTS AND DISCUSSION

The morphology of the obtained Pd nanostructures was investigated by scanning electron microscope (SEM), as shown in Fig. 1 (a-d). At a low resolution (Fig. 1a), the overall Pd structures resemble a large sheet on the scale of sub-millimeters. The details of the morphology were revealed by a high-resolution image (Fig. 1b), which corresponds to the white marked region in Fig. 1a. This top view allows us to discern the delicate structures; the large sheets are actually made up of a great number of tiny nanofibers (around 70/μm^2) uprightly aligning with each other. The side views (Fig. 1c and 1d) show that three portions constitute an indivisible whole: a layer formed by partly connected particles with a diameter of 1 μm on the top (Fig. 1c), NFAs with a diameter of 100 ~ 160 nm and a length of 8 μm in the middle (Fig. 1c), and a firm sheet with a thickness of 2 μm on the bottom (Fig. 1d). The structure is schematically illustrated in the upper inset in Fig. 1. For the architectural designs in reality, the presence of beams significantly enhances the anti-deformation ability of pillars (the lower inset in Fig. 1). Accordingly, with the assistance of the top and bottom supporting layers in the Pd nanostructures, every Pd nanofiber with fairly long length is spatially fixed and vertically aligning together without aggregation, so that the large surface area of nanofibers is well conserved. Furthermore, the incomplete connection of particles on the top layer leaves gaps between them, which could become diffusion tunnels for reactants and products in catalytic applications. The durability of the Pd NFAs

was checked by SEM and the result is shown in Fig. S3. After 7 months of conservation in DCM, the Pd NFAs still orderly arranged and well isolated with each other, and their original morphology is well maintained without aggregation. The X-ray diffraction (XRD) pattern of the deposits (Fig. S1) only shows the diffraction peaks of metallic Pd. The energy dispersive x-ray spectrometer (EDX) analysis (Fig. S2), performed simultaneously with SEM measurements, detected only X-ray fluorescence of Pd. These results confirmed that the deposits are composed of Pd metal.

To investigate the morphology variation of the Pd NFAs during the formation, the synthesis was terminated at different reaction periods. Fig. 2 (a-d) shows the SEM images of the Pd nanostructures with the reaction times (t) of 1, 4, 12, and 20 h respectively, and the corresponding morphology schematics are shown as insets at the bottom left of each SEM image. At t = 1 h, short nanofibers with small particles at the tip were found as the deposit, demonstrating that the nanofibers and particles are formed at the initial stage and growing simultaneously. When t = 4 h (Fig. 2b), the same structures were obtained except that the size is larger than that at t = 1 h, indicating that the particles and nanofibers were growing during this period. However, no bottom layers can be found in Fig. 2a and 2b, resulting in randomly agglomerated nanofibers due to the absence of bottom immobilization. At t = 12 h, as shown in Fig. 2c, the neatly ordered arrangement of the Pd NFAs can be clearly observed through the bottom side, and the small interlinked sheets

perfectly exhibit how the bottom supporting layers are formed during this period. Unexpectedly, the growth of three portions proceeds segmentally, and the formation of bottom supporting layers is later than that of particles and nanofibers. When t = 20 h (Fig. 2d), the Pd NFAs with three portions have been finally formed. It can be observed that the size of nanofibers and particles at t = 20 h (Fig. 2d) remain unchanged compared with that at t = 12 h (Fig. 2c), while the interlinked bottom supporting layers have grown to complete layers. The SEM results reveal that at a certain time, the growth of nanofibers ends, whereas the formation of bottom supporting layers starts.

Our previous studies have demonstrated that the IL|W interface can be applied for the preparation of noble metal nanofibers, and that both of the high viscosity[58] of IL and IL itself contribute to induce the formation of such 1D nanostructures.[53-55] In the case of Pt nanofibers,[55] we confirmed a structure combining two kinds of morphology together, that is, nanofibers with particles at the tip. It was verified that such morphology results from an interfacial growth of Pt metal towards W as particles, and towards IL as nanofibers simultaneously.[55] The great distinction of growth environment of metal nanostructures in W and IL gives rise to the utterly different morphology of the metal formed on each liquid side of the RAIL|W interface but combine together as a whole. Therefore, it is quite reasonable to presume that the Pd nanofibers and particles are formed on the RAIL and W sides of the RAIL|W interface respectively for the present case. Nevertheless, the

formation of a new shape, the sheet at the bottom, is likely to be caused by the growth in a non-uniform media, implying the growth environment for Pd on the RAIL side of the RAIL | W interface changes drastically during the reaction period.

By visually observing the reaction system at different reaction times (Fig. S4), we noticed that the color of W changed from yellow, which originates from initially dissolved $PdCl_4^{2-}$, to dark green. Fig. S5 shows the UV-vis spectra for the aqueous solutions before and after a typical synthesis of the Pd NFAs for 20 h, and a $FcMDDA^{2+}$ solution as a comparison. The solution before the reaction shows a peak at 425 nm which is ascribable to $PdCl_4^{2-}$.[59] The peak vanished after the reaction, indicating that $PdCl_4^{2-}$ ions have been consumed after the 20 h reaction. The spectrum after the reaction shows a new peak at 627 nm attributable to $FcMDDA^{2+}$, which is generated due to the oxidation of $FcMDDA^{+}$ by the ET reaction (eqn 1),

$$2FcMDDA^{+}\,(RAIL) + PdCl_4^{2-}\,(W) \rightarrow 2FcMDDA^{2+}\,(RAIL) + Pd + 4Cl^{-}\,(W) \quad (1)$$

The absorption peak for $FcMDDA^{2+}$ observed in W after the reaction demonstrates that $FcMDDA^{2+}$ have transferred from RAIL to W (eqn 2).

$$FcMDDA^{2+}\,(RAIL) \rightarrow FcMDDA^{2+}\,(W) \quad (2)$$

These processes were actually confirmed by applying liquid-liquid electrochemistry at the IL|W interface using micropipettes[60, 61] to the present RAIL|W interface (Supporting Information, Fig. S12).

In our preceding reports,[53-55] we have revealed and discussed the detailed mechanism about the metal nanostructures formed by the spontaneous redox reaction at the IL|W interface. Unlike a single phase reaction, the separation of reductant and oxidant in IL and W spatially confines the redox reaction only taking place at the IL|W interface. Moreover, the ET taking place across the IL|W interface leads to unbalanced charges in IL and W. Therefore, another charge transfer with the opposite direction of ET is indispensable, for neutralizing the excess charges in each liquid phase. In the previous cases for Au and Pt nanofibers, the ET is commonly coupled with the IT of the metal precursors ($AuCl_4^-$ and $PtCl_4^{2-}$) from W to IL, in order to balance the electroneutrality of each IL and W phase. In the present case, the UV-vis (Fig. S5) and electrochemistry (Fig. S12) results demonstrate that the IT of $FcMDDA^{2+}$ (eqn 2) occurs and is coupled with ET, but the IT of $PdCl_4^{2-}$ still may occur (eqn 3).

$$PdCl_4^{2-}(W) \rightarrow PdCl_4^{2-}(RAIL) \quad (3)$$

The IT of $PdCl_4^{2-}$ cannot be measured for the RAIL-W system since the ET between $PdCl_4^{2-}$ and $FcMDDA^+$ (eqn 1) is inevitable and hinders the IT

measurements. Therefore, it is difficult to directly compare the standard IT potentials for $PdCl_4^{2-}$ and $FcMDDA^{2+}$ in the RAIL-W system. Instead, we used a redox-inactive IL trihexyltetradecylphosphonium tetrakis(3,5-bis(trifluoromethyl)phenyl)borate ($[THTDP^+][TFPB^-]$) to investigate the relative hydrophobicity of $PdCl_4^{2-}$ and $FcMDDA^{2+}$ in the IL-W system. The CVs for the IT across the IL|W interface (Fig. S14) display that the midpoint potential (E_{mid}) of the IT of $FcMDDA^{2+}$ is 290 mV more positive than that of $PdCl_4^{2-}$ (see Supporting Information for the detailed discussion).

The above results mean that the IT of $FcMDDA^{2+}$ from IL to W is more thermodynamically favored than the IT of $PdCl_4^{2-}$ from W to IL. It implies that the latter does not occur also at the RAIL|W interface. However, the morphology of the Pd NFAs contradicts with the implication. Since W is a homogeneous and low-viscosity media, the segmented structures are unlikely to be completely formed only on the W side of the RAIL|W interface. However, the growth of Pd on the RAIL side of the RAIL|W interface requires Pd precursor ($PdCl_4^{2-}$) in RAIL and, therefore, inevitably needs the IT of $PdCl_4^{2-}$ from W to RAIL as the necessary condition. Actually, the CVs at the IL|W interface (Fig. S14) do not reflect the reaction condition at the RAIL|W interface. In the present case, without the IT of $PdCl_4^{2-}$, the IT of $FcMDDA^{2+}$ (eqn 2) can initiate the interfacial redox reaction by coupling with the ET (eqn 1):

$$2FcMDDA^{+}\,(RAIL) + PdCl_4^{2-}\,(W) \rightarrow FcMDDA^{2+}\,(W) + FcMDDA^{2+}\,(RAIL) + Pd + 4Cl^{-}\,(W) \quad (4)$$

With the reaction proceeding, half of the generated $FcMDDA^{2+}$ remains inside the RAIL (eqn 4). They should have been gradually diffused to the RAIL bulk, which would result in the color change of RAIL just as W. However, the RAIL bulk maintained the original color after the 20 h reaction (Fig. S4), indicating that the $FcMDDA^{2+}$ on the RAIL side of the RAIL|W interface were not diffused to the RAIL bulk. This could be explained by thin diffusion layer; the thickness of the diffusion layer was estimated to be 400 μm, from $\sqrt{D^{\mathrm{RAIL}}t}$ with $D^{\mathrm{RAIL}} = 2 \times 10^{-12}$ m^2s^{-1} and $t = 20$ h. Here, the diffusion coefficient of $FcMDDA^{2+}$ in RAIL, D^{RAIL}, was estimated using $D^{\mathrm{RAIL}}\eta^{\mathrm{RAIL}} = D^{\mathrm{W}}\eta^{\mathrm{W}}$ from the Stokes-Einstein equation and we used $\eta^{\mathrm{RAIL}} = 430$ mPa·s at 70 °C (measured) and typical values for $D^{\mathrm{W}} = 1\times 10^{-9}$ m^2s^{-1} and $\eta^{\mathrm{W}} = 1$ mPa·s as a reference condition. Therefore, an intermediate layer enriched with $FcMDDA^{2+}$ is formed by the accumulation of the $FcMDDA^{2+}$ on the RAIL side of the RAIL|W interface on account of the slow diffusion rate. The IT of $PdCl_4^{2-}$ from W to the RAIL bulk may be unfavorable as in the IL-W system (Fig. S14), however, the IT of $PdCl_4^{2-}$ from W to the intermediate layer can be facilitated by the accumulated $FcMDDA^{2+}$ because of the strong electrostatic interaction between the two divalent ions. Unlike the relatively long Au and Pt nanofibers with the length of several tens micrometers formed on the IL side of the

IL|W interface,[53-55] the nanofibers in the Pd NFAs is only 8 micrometers in the length. The Au and Pt nanofibers can grow to such long length due to a favored IT of metal precursors ($AuCl_4^-$ and $PtCl_4^{2-}$) from W to the IL bulk, but the relatively short length of nanofibers in the Pd NFAs implies that the transfer of $PdCl_4^{2-}$ from W to the RAIL bulk is restricted.

According to the above discussion, the IT of $FcMDDA^{2+}$ from RAIL to W and the IT of $PdCl_4^{2-}$ from W to RAIL (limited in the intermediate layer) should both occur and contribute to be coupled with ET together. After 20 h reaction, the concentration of the transferred $FcMDDA^{2+}$ in W was estimated from the absorbance and the molar absorptivity 560 $M^{-1}cm^{-1}$ at 627 nm (Fig. S5). The concentration was found to be 4.8 mM, which is approximately half of 10 mM, the initial concentration of $PdCl_4^{2-}$ in W.

Based on the finding that the ratio of the concentration of $FcMDDA^{2+}$ after the reaction in W on that of $PdCl_4^{2-}$ before the reaction is half, it can be known that both IT of eqns 2 and 3 contribute to be coupled with ET with the contribution ratio of 2: 1, and thus the total interfacial reaction can be written：

$$6FcMDDA^{+}\,(RAIL) + 4PdCl_4^{2-}\,(W) \rightarrow 4FcMDDA^{2+}\,(RAIL) + 3Pd + 12Cl^{-}\,(W) + 2FcMDDA^{2+}\,(W) + PdCl_4^{2-}\,(RAIL) \quad (5)$$

In order to observe the RAIL|W interface before and after the reaction with a

resolution higher than the visual observation (Fig. S4), a miniature reaction system was prepared by dropping RAIL and W on a glass slide capped with glass cover on the top. Before the reaction, the RAIL|W interface can be clearly observed in the photograph (Fig. S6a). However, after 20 h reaction (Fig. S6b), a legible dark green circle corresponding to the $FcMDDA^{2+}$ enriched layer appeared whose thickness was measured to be several tens micron with the photograph resolution. The corresponding microscope images taking with a reflected light microscope (Fig. S7) reveal that an intermediate layer containing the metal deposit inside (silver white) is formed between W and RAIL after 20 h reaction (Fig. S7b) compared with the initial state (Fig. S7a). The thickness of this intermediate layer is around 20 μm, which is comparable with the length of Pd NFAs found in the SEM images (Fig. 1). The above results support the existence of the intermediate layer.

Based on the above discussion, a possible mechanism for the spontaneous growth of Pd NFAs can be inferred. As illustrated in Fig. 3, at the first stage, the interfacial ET reaction (eqn 1) occurs by coupling with the IT of $FcMDDA^{2+}$ from RAIL to W (eqn 2), and an intermediate layer is gradually formed by the accumulation of $FcMDDA^{2+}$ remained inside RAIL. The IT of PdC_4^{2-} from W to the $FcMDDA^{2+}$ enriched intermediate layer is facilitated by the strong electrostatic interaction between the two divalent ions. The $PdCl_4^{2-}$ remained in W and transferred into the intermediate layer will be the reactants for growing Pd metal

on the W side as particles and on the RAIL side as nanofibers, respectively, the latter of which is like the case of Pt nanofibers.[55] At the second stage, when all of $PdCl_4^{2-}$ ions in W were depleted owing to ET (eqn. (1)) and IT (eqn. (3)), the growth of particles on the W side has to cease since no Pd precursor in W anymore, but the $PdCl_4^{2-}$ in the intermediate layer still can react with $FcMDDA^+$ that is supplied from RAIL bulk. Nevertheless, when the nanofibers grow until the bottom of the intermediate layer, the growth environment changes drastically, altering the growing model from 1D nanofiber to 2D sheet. As a result, Pd sheets were formed at the end of nanofibers at the bottom of the intermediate layer.

A question is why all the nanofibers in the Pd NFAs grow vertically. Some 1D nanostructures are reported to be adsorbed at the liquid/liquid interface with a horizontal orientation because of the lower net surface energy.[62] However, regarding metallic 1D nanostructures, the orientation at the liquid/liquid interface has not been fully revealed, although it has been tackled by some researchers.[63, 64] For the 1D nanofiber parts of the Pd NFAs in the present study, the SEM images in Fig.1 clearly show that they are vertically orientated. In the present study, the W and the RAIL phases are separated by the formed intermediate layer whose thickness gradually increases with time. The growth of particles on the W side is realized by the electrons delivered inside the Pd metal rather than the direct contact between $PdCl_4^{2-}$ and reducing agent (redox-active cation $FcMDDA^+$). However, the concentration of the reducing agent on the RAIL side of the RAIL | W interface

drastically decreases because of the consumption due to the redox reaction and also the accumulated $FcMDDA^{2+}$ in the intermediate layer. The vertical growth of Pd nanofibers inside the intermediate layer is promoted in such a condition, so as to reach a faster reaction rate by keeping the contact of the Pd metal surface with reducing agent in a higher concentration. This is the idea proposed by Hasse *et al.*, when they obtained Ag wires at the O|W interface.[58]

Two control experiments were performed to authenticate the indispensable role the redox-active cation $FcMDDA^+$ played in the present study. First, the IL cation $FcMDDA^+$ was replaced by a redox-inactive cation, trioctylmethylammonium ($TOMA^+$), and decamethylferrocene (DMFc) was added as the reducing agent in the IL $[TOMA^+][C_4C_4N^-]$. For this case using $[TOMA^+][C_4C_4N^-]$ instead of $[FcMDDA^+][C_4C_4N^-]$, only Pd nanofibers with homogeneous shape was obtained as a product (Fig. S8a). The absence of disparate parts in the Pd structure for the $[TOMA^+][C_4C_4N^-]$ case confirms that the use of $FcMDDA^+$ is essential for the formation of vertically aligned Pd NFAs. The concentration gradient of the redox couple $DMFc/DMFc^+$ caused by the slow diffusion rate in $[TOMA^+][C_4C_4N^-]$ cannot induce such segmented morphology, which indirectly proved the possibility of the formation of the intermediate layer. Second, the IL anion $C_4C_4N^-$ was replaced to a highly hydrophobic anion tetrakis[3,5-bis(trifluoromethyl)phenyl]borate ($TFPB^-$), and the RAIL $[FcMDDA^+][TFPB^-]$[56, 57] was adopted as the hydrophobic liquid phase in the

system as a comparison. As shown in Fig. S8b and S8c, except for the shorter length of nanofibers, the resultant product possesses the analogous structure with three distinctive portions, particles on the top, nanofibers in the middle and firm sheet at the bottom, which demonstrates that the reason for giving rise to such kind of structure is the use of $FcMDDA^+$. The above results reveal that the $FcMDDA^+$ is crucial for the formation of the intermediate layer and vertically aligned Pd NFAs.

Since the RAIL with extraordinarily high concentration of reducing agent was adopted as the hydrophobic liquid phase in the present study, the surface density of formed Pd nuclei at the RAIL|W interface will be adjusted by the concentration of $PdCl_4^{2-}$ which is oxidizing agent in W. Hence, in order to manifest the role of the top supporting layer constituted with connected particles, we decreased the initial concentration of $PdCl_4^{2-}$, which will result in lowered nuclei density of Pd and enlarged distance between each particle at the RAIL|W interface. Pd nanostructures were prepared with the concentration of $PdCl_4^{2-}$ in W decreased from 10 mM to 5 mM while the other conditions remained unchanged. The results are shown in Fig. 4 (a-d). Surprisingly, when the concentration of $PdCl_4^{2-}$ is reduced by half, all Pd nanofibers lie down (Fig. 4c) rather than stand vertically (Fig. 4a) (more detailed SEM images showing the difference are in Fig. S9). Fig 4d distinctly shows that the bottom sheets were still formed in this condition. This phenomenon can be explained by the schematics of Fig. 4e and 4f. The density of

Pd nuclei decreases as the concentration of $PdCl_4^{2-}$ decreases, and the distance between neighboring nuclei is so large that the particles cannot horizontally connect with each other. Therefore, the failure of the vertical arrangement of nanofiber arrays attributes to the absence of the top supporting layer. The above results demonstrate that only the bottom supporting layer is insufficient to make such long nanofibers vertically aligned, and that the construction of the top supporting layer is indispensable for stabilizing the vertical arrangement of Pd nanofibers. In another control experiment, the RAIL was diluted with the $[TOMA^+][C_4C_4N^-]$ to the concentration of 0.5 M (Fig. S10a and 10b) or 0.1 M (Fig. S10c and 10d). We obtained Pd nanostructures basically the same as the Pd NFAs, however, the nanofibers are not as orderly aligned as the Pd NFAs. With the decrease in the concentration of the reducing agent, the Pd nanofibers cannot grow as steadily as the case of Pd NFAs. The results indicate that the formation of highly ordered Pd NFAs needs a high concentration of the reducing agent.

The application performance of Pd NFAs for direct ethanol fuel cell was investigated by measuring the electrocatalytic activity of Pd NFAs toward ethanol oxidation reaction (EOR) in an alkaline media, and the commercial Pd/C catalyst was also measured as a comparison. Fig. 5a shows cyclic voltammograms (CVs) for Pd NFAs and Pd/C catalysts in a N_2-purged 1 M NaOH solution. The electrochemically active surface area (EASA) of the catalyst was estimated from the charge of the reduction peak at $E \approx -0.45$ V. The EASA of Pd NFAs was found

to be 38 m^2/g, which is around 53% of the Pd/C catalyst (72 m^2/g). The relatively lower EASA for Pd NFAs is likely due to the intrinsic 1D morphology of NFAs compared with 0D morphology of nanoparticles. The EOR curves of Pd NFAs and Pd/C catalysts were recorded by CV measurements in a 1 M Na OH + 1 M ethanol solution at the scan rate of 50 mV/s, and then normalized by the EASA of Pd (Fig. 5b). The oxidation peak in the forward scan (I_f) corresponds to the oxidation of adsorbed ethanol, while the oxidation peak in the backward scan (I_b) is associated with the oxidation of residual carbonaceous species adsorbed on the Pd surface. The results indicate that Pd NFAs present a comparable specific activity with Pd/C toward EOR on account of similar onset potentials and a higher I_f (1.71 mA/cm^2) compared with that of Pd/C (1.66 mA/cm^2). In addition, the I_f/I_b ratio can be an index of the catalytic tolerance toward the carbonaceous species accumulated on the surface of the electrode.[65] Pd NFAs (0.87) exhibits higher I_f/I_b ratio than Pd/C (0.80), manifesting a more effective removal of poisoning species on the catalyst surface. Furthermore, chronoamperometry (CA) measurements were conducted in a 1 M NaOH + 1 M ethanol solution at an applied voltage of −0.3 V in order to investigate the catalytic stability of Pd NFAs and Pd/C, and the results are shown in Fig. 5c. The currents for the two catalysts both decayed rapidly at the initial period, which can be ascribed to surface poisoning by the accumulation of adsorbed reaction intermediates on the active sites, and reached the pseudo-steady state at 2000 s (I_s). Pd NFAs exhibit a higher initial current and a 1.25 times higher

I_s (0.23 mA/cm^2) compared that of Pd/C (0.18 mA/cm^2), illustrating better durability for EOR in alkaline media. Although the EASA of Pd NFAs is smaller than that of Pd/C, the better electrocatalytic performance of Pd NFAs towards EOR can be explained by the following two aspects. First, the incomplete connection of the particles constituting the top supporting layer bear the Pd nanofibers vertically aligned. Such kind of structure not only conserves the high surface area of Pd nanofibers but also remains deep hollows between nanofibers, which can be numerous diffusing channels for the reactant and product. Therefore, the reaction species can diffuse in and out from the channels easily. Second, the top-middle-bottom structures are all made of Pd, which is beneficial for the charge transfer during electrochemical reactions by forming fully conductive frameworks. The stability of Pd NFAs was investigated by CVs in a 1 M NaOH + 1 M ethanol solution at 50 mV/s for 10-time cycles, which are shown in Fig. 5d. The peak current density only decreases 3.5% at the tenth scan compared with that at the first scan, indicating a good stability of Pd NFAs towards EOR.

CONCLUSIONS

Vertically aligned Pd NFAs with three portions (particles, NFAs, sheets) have been prepared by applying the RAIL|W interface as a formation site, where the use of the template is not required. The oxidized cation $FcMDDA^{2+}$, which is generated via ET between $FcMDDA^{+}$ and $PdCl_4^{2-}$ ions, not only plays a role of the

source of IT to balance the excess charges brought by ET, but also forms an intermediate layer between W and RAIL, making possible the formation of different structural units, and the connection between them together. With the assistance of the top supporting layer formed by the connection between particles, Pd nanofibers with a height reaching several micrometers still can vertically stand, and thus the large surface area of the nanofibers is highly conserved. The aggregation of the Pd nanofibers was restrained in a liquid environment by the immobilization of 1D units on the bottom supporting layer. The EOR measurements revealed that Pd NFAs can be applied for direct ethanol fuel cell due to its large surface area, definite 1D electron conductivity, and high durability.

EXPERIMENTAL SECTION

Preparation of Pd NFAs

In a typical synthesis, 2 mL of water containing HCl (0.1 M) and H_2PdCl_4 (0.01 M) was poured onto 0.2 g of RAIL $[FcMDDA^+][C_4C_4N^-]$ (synthesis method is in Supporting Information) in a 3 mL glass bottle, to form the RAIL|W interface. The RAIL acts as the reducing agent as well as the hydrophobic liquid phase simultaneously in the two-phase system. Then the glass bottle was put in an oil bath at 70 ^oC for 20 h. Black deposits that were spontaneously formed at the RAIL|W interface were washed by a mixed solvent (50:50 vol %) of methanol and dichloromethane (DCM) to remove the residual IL over 5 times.

Evaluation of electrocatalytic activity

Electrocatalytic measurements were performed on an electrochemical working station by using a three-electrode system at room temperature (25 ^{o}C), including a catalyst-loaded glassy carbon working electrode (GCE), a saturated calomel reference electrode (SCE) and a Pt foil counter electrode.

(1) Loading catalysts on GCE

A GCE surface with a diameter of 3 mm and a geometric area of 0.071 cm^2 was polished with Al_2O_3 particle suspension and then dried at room temperature in air after rinsing with Milli-Q water. Pd NFAs or Pd/C (Sigma-Aldrich, Palladium on activated charcoal, 10% Pd basis) catalysts were loaded by casting 5 μL of Pd NFAs or 10 μL Pd/C dispersed ethanol solution (1mg/mL) on the GCE surface. 10 μL of 0.05 wt% Nafion/ethanol solution was dropped onto the catalyst-loaded GCE surfaces in order to protect Pd NFAs or Pd/C catalyst films.

(2) Measurement for electrochemically active surface area (EASA) of catalysts

CVs were recorded in a 1 M deoxygenated NaOH solution from −1.0 V to 0.6 V at a scan rate of 50 mV/s. The EASA of Pd NFAs or Pd/C catalysts was evaluated the integration of the current at the PdO reduction region in the cathodic scan, assuming a value of 405 μC/cm^2 for the reduction of Pd monolayer as previously reported.[66]

(3) Electrocatalytic measurements of catalysts

CV and CA measurements were conducted in a deoxygenated 1 M NaOH + 1 M ethanol solution at a scan range of −0.9~0.1 V and an applied voltage of −0.3

V for 2000 s, respectively.

ACKNOWLEDGMENT

This work was financially supported by JSPS KAKENHI (No. 18K05171).

ASSOCIATED CONTENT

Supporting Information Available: detailed information on materials and methods. XRD patterns of the Pd NFAs. SEM image and EDX elemental mapping of Pd for the NFAs. SEM images for the Pd NFAs that are conserved in DCM for 7 months. Photos of the RAIL-W two-phase reaction systems at different reaction times. UV-vis spectra for the aqueous solutions before and after 20 h reaction. Photographs and optical microscope images of a miniature reaction system for the RAIL|W interface before and after 20 h reaction. SEM images of the Pd nanostructures obtained by the same reaction conditions with the typical synthesis of Pd NFAs except for replacing the IL from $[FcMDDA^+][C_4C_4N^-]$ to a redox-inactive IL, $[TOMA^+][C_4C_4N^-]$, with an addition of DMFc as the reducing agent and another RAIL, $[FcMDDA^+][TFPB^-]$. SEM images showing details of the Pd NFAs. The cell configurations for the electrochemical measurements. CVs at the RAIL|W interface for the IT of $FcMDDA^{2+}$, the potential window of $[FcMDDA^+][C_4C_4N^-]$ and the ET between $PdCl_4^{2-}$ and $FcMDDA^+$. CVs of Pd NFAs and Pd/C in a 1 M NaOH solution at 50 mV/s. CVs of Pd NFAs and Pd/C

in a 1 M NaOH + 1 M ethanol solution at 50 mV/s. CAs of Pd NFAs and Pd/C in a 1 M NaOH + 1 M ethanol solution at an applied voltage of –0.3 V for 2000 s. This material is available free of charge via the Internet at http://pubs.acs.org.

AUTHOR INFORMATION

Corresponding Author

Naoya Nishi: nishi.naoya.7e@kyoto-u.ac.jp

ORCID

Tetsuo Sakka: 0000-0002-1892-8056

Naoya Nishi: 0000-0002-5654-5603

REFERENCES

[1] Zhang, J. Z.; Noguez, C. Plasmonic Optical Properties and Applications of Metal Nanostructures. *Plasmonics* **2008**, *3*, 127-150.

[2] Liu, H. L.; Nosheen, F.; Wang, X. Noble Metal Alloy Complex Nanostructures: Nontrollable Synthesis and their Electrochemical Property. *Chem. Soc. Rev.* **2015**, *44*, 3056-3078.

[3] Mohanty, A.; Garg, N.; Jin, R., A Universal Approach to the Synthesis of Noble Metal Nanodendrites and their Catalytic Properties. *Angew Chem. Int. Ed. Engl.* **2010**, *49*, 4962-4966.

[4] Tao, A. R.; Habas, S.; Yang, P. Shape Control of Colloidal Metal Nanocrystals. *Small* **2008**, *4*, 310-325.

[5] Zeng, J.; Zheng, Y.; Rycenga, M.; Tao, J.; Li, Z.; Zhang, Q.; Zhu, Y.; Xia, Y. Controlling the Shapes of Silver Nanocrystals with Different Capping Agents. *J. Am. Chem. Soc.* **2010**, *132*, 8552-8553.

[6] Quintanilla, A.; Butselaar-Orthlieb, V. C. L.; Kwakernaak, C.; Sloof, W. G.; Kreutzer, M. T.; Kapteijn, F. Weakly Bound Capping Agents on Gold Nanoparticles in Catalysis: Surface Poison? *J. Catal.* **2010**, *271*, 104-114.

[7] Shi, H.; Qi, L.; Ma, J.; Wu, N. Architectural Control of Hierarchical Nanobelt Superstructures in Catanionic Reverse Micelles. *Adv. Funct. Mater.* **2005**, *15*, 442-450.

[8] Xiong, S.; Xi, B.; Wang, C.; Xu, D.; Feng, X.; Zhu, Z.; Qian, Y. Tunable Synthesis of Various Wurtzite ZnS Architectural Structures and Their Photocatalytic Properties. *Adv. Funct. Mater*. **2007**, *17*, 2728-2738.

[9] Yu, Y.; Zhang, Q.; Xie, J.; Lee, J. Y. Engineering the Architectural Diversity of Heterogeneous Metallic Nanocrystals. *Nat. Commun.* **2013**, *4*, 1454-1462.

[10] Wang, X.; Song, J.; Wang, Z. L. Nanowire and Nanobelt Arrays of Zinc Oxide from Synthesis to Properties and to Novel Devices. *J. Mater. Chem.* **2007**, *17*, 711-720.

[11] Chen, Y.; Milenkovic, S.; Hassel, A. W. Arrays of Iso-Oriented Gold Nanobelts. *Nano lett.* **2008**, *8*, 737-742.

[12] Peng, K.; Xu, Y.; Wu, Y.; Yan, Y.; Lee, S. T.; Zhu, J. Aligned Single-

Crystalline Si Nanowire Arrays for Photovoltaic Applications. *Small* **2005,** *1*, 1062-1067.

[13] Huang, Z.; Fang, H.; Zhu, J. Fabrication of Silicon Nanowire Arrays with Controlled Diameter, Length, and Density. *Adv.Mater.* **2007**, *19*, 744-748.

[14] Hochbaum, A. I.; Fan, R.; He, R.; Yang, P. Controlled Growth of Si Nanowire Arrays for Device Integration. *Nano lett.* **2005**, *5*, 457-460.

[15] Nguyen-Vu, T. D.; Chen, H.; Cassell, A. M.; Andrews, R.; Meyyappan, M.; Li, J. Vertically Aligned Carbon Nanofiber Arrays: an Advance toward Electrical-Neural Interfaces. *Small* **2006,** *2*, 89-94.

[16] Jennings, J. R.; Ghicov, A.; Peter, L. M.; Schmuki, P.; Walker, A. B. Dye-Sensitized Solar Cells Based on Oriented TiO_2 Nanotube Arrays: Transport, Trapping, and Transfer of Electrons. *J. Am. Chem. Soc.* **2008**, *130*, 13364–13372.

[17] Dávila, D.; Tarancón, A.; Calaza, C.; Salleras, M.; Fernández-Regúlez, M.; San Paulo, A.; Fonseca, L. Monolithically Integrated Thermoelectric Energy Harvester Based on Silicon Nanowire Arrays for Powering Micro/nanodevices. *Nano Energy* **2012**, *1*, 812-819.

[18] Yamada, Y. M.; Yuyama, Y.; Sato, T.; Fujikawa, S.; Uozumi, Y. A Palladium-Nanoparticle and Silicon-Nanowire-Array Hybrid: A Platform for Catalytic Heterogeneous Reactions. *Angew. Chem. Int. Ed.* **2014**, *53*, 127-131.

[19] Saedi, A.; Ghorbani, M. Electrodeposition of Ni–Fe–Co Alloy Nanowire In Modified AAO Template. *Mater. Chem. Phys.* **2005**, *91*, 417-423.

[20] Sun, X.-Y.; Xu, F.-Q.; Li, Z.-M.; Zhang, W.-H. Cyclic Voltammetry for the Fabrication of High Dense Silver Nanowire Arrays with the Assistance of AAO Template. *Mater. Chem. Phys.* **2005**, *90*, 69-72.

[21] Kim, K.; Kim, M.; Cho, S. M. Pulsed Electrodeposition of Palladium Nanowire Arrays Using AAO Template. *Materials Mater. Chem. Phys.* **2006**, *96*, 278-282.

[22] Wang, X.; Wang, X.; Huang, W.; Sebastian, P. J.; Gamboa, S. Sol–Gel Template Synthesis of Highly Ordered MnO_2 Nanowire Arrays. *J. Power Sources* **2005**, *140*, 211-215.

[23] Zhao, S.; Roberge, H.; Yelon, A.; Veres, T. New Application of AAO Template: A Mold for Nanoring and Nanocone Arrays. *J. Am. Chem. Soc.* **2006**, *128*, 12352-12353.

[24] Schlossman, M. L. X-Ray Scattering from Liquid–Liquid Interfaces. *Physica B* **2005**, *357*, 98–105.

[25] Brust, M.; Walker, M.; Bethell, D.; Schiffrin, D.; Whyman, R. Synthesis of Thiol-Derivatised Gold Nanoparticles In a Two-Phase Liquid–Liquid System. *J. Chem. Soc., Chem. Commun.* **1994**, 801-802.

[26] Rao, C. N. R.; Kulkarni, G. U.; Thomas, P. J.; Agrawal, V.V.; Saravanan, P. Films of Metal Nanocrystals Formed at Aqueous-Organic Interfaces. *J.*

Phys. Chem. B **2003**, *107*, 7391-7395.

[27] Booth, S. G.; Uehara, A.; Chang, S. Y.; Mosselmans, J. F. W.; Schroeder, S. L. M.; Dryfe, R. A. W. Gold Deposition at a Free-Standing Liquid/Liquid Interface: Evidence for the Formation of Au(I) by Microfocus X-ray Spectroscopy (μXRF and μXAFS) and Cyclic Voltammetry. *J. Phys. Chem. C* **2015**, *119*, 16785-16792.

[28] Gründer, Y.; Fabian, M. D.; Booth, S. G.; Plana, D.; Fermín, D. J.; Hill, P. I.; Dryfe, R. A. W. Solids at The Liquid–Liquid Interface: Electrocatalysis With Pre-Formed Nanoparticles. *Electrochim. Acta* **2013**, *110*, 809-815.

[29] Rao, C. N. R.; Kalyanikutty, K. P. The Liquid–Liquid Interface as a Medium To Generate Nanocrystalline Films of Inorganic Materials. *Accounts Chem. Res.* **2008**, *41*, 489-499.

[30] Trojánek, A.; Langmaier, J.; Samec, Z. Electrocatalysis of the Oxygen Reduction at a Polarised Interface Between Two Immiscible Electrolyte Solutions By Electrochemically Generated Pt Particles. *Electrochem. Commun.* **2006**, *8*, 475-481.

[31] Zhu, X.; Qiao, Y.; Zhang, X.; Zhang, S.; Yin, X.; Gu, J.; Chen, Y.; Zhu, Z.; Li, M.; Shao, Y. Fabrication of Metal Nanoelectrodes By Interfacial Reactions. *Anal. Chem.* **2014**, *86*, 7001-7008.

[32] Mirčeski, V.; Gulaboski, R. Simple Electrochemical Method for Deposition and Voltammetric Inspection of Silver Particles at the Liquid-Liquid

Interface of a Thin-Film Electrode*J. Phys. Chem. B* **2006**, *110*, 2812-2820.

[33] Sakata, J. K.; Dwoskin, A. D.; Vigorita, J. L.; Spain, E. M. Film Formation of Ag Nanoparticles at the Organic-Aqueous Liquid Interface. *J. Phys. Chem. B* **2005**, *109*, 138-141.

[34] Guo, J.; Tokimoto, T.; Othman, R.; Unwin, P. R. Formation of Mesoscopic Silver Particles at Micro and Nano-Liquid/Liquid Interfaces. *Electrochem. Commun.* **2003**, *5*, 1005-1010.

[35] Aslan, E.; Patir, I. H.; Ersoz, M. Cu Nanoparticles Electrodeposited at Liquid-Liquid Interfaces: A Highly Efficient Catalyst for the Hydrogen Evolution Reaction. *Chemistry* **2015**, *21*, 4585-4589.

[36] Agrawal, V. V.; Mahalakshmi, P.; Kulkarni, G. U.; Rao, C. N. R. Nanocrystalline Films of Au-Ag, Au-Cu, and Au-Ag-Cu Alloys Formed at the Organic-Aqueous Interface. *Langmuir*, **2006**, *22*, 1846-1851.

[37] Izquierdo, D.; Martinez, A.; Heras, A.; Lopez-Palacios, J.; Ruiz, V.; Dryfe, R. A.; Colina, A. Spatial Scanning Spectroelectrochemistry. Study of the Electrodeposition of Pd Nanoparticles at the Liquid/Liquid Interface. *Anal. Chem.* **2012**, *84*, 5723-5730.

[38] Lee, W. P.; Chen, H.; Dryfe, R.; Ding, Y. Kinetics of Nanoparticle Synthesis By Liquid–Liquid Interfacial Reaction. *Colloids and Surfaces A: Physicochem. Eng. Aspects* **2009**, *343*, 3-7.

[39] Dutta, S.; Sarkar, S.; Ray, C.; Roy, A.; Sahoo, R.; Pal, T. Mesoporous Gold

and Palladium Nanoleaves from Liquid-Liquid Interface: Enhanced Catalytic Activity of the Palladium Analogue toward Hydrazine-Assisted Room-Temperature 4-Nitrophenol Reduction. *ACS Appl. Mater. Interfaces* **2014**, *6*, 9134-43.

[40] Johans, C.; Lahtinen, R.; Kontturi, K.; Schiffrin, D. J. Nucleation at Liquid|Liquid Interfaces: Electrodeposition without Electrodes. *J. Electroanal. Chem.* **2000**, *488*, 99-109.

[41] Johans, C.; Kontturi, K.; Schiffrin, D. J. Nucleation at Liquid|Liquid Interfaces: Galvanostatic Study. *J. Electroanal. Chem.* **2002**, *526*, 29-35.

[42] Lahtinen, R. M.; Fermín, D. J.; Jensen, H.; Kontturi, K.; Girault, H. H. Two-Phase Photocatalysis Mediated by Electrochemically Generated Pd Nanoparticles. *Electrochem. Commun.* **2000**, *2*, 230-234.

[43] Platt, M.; Dryfe, R. A. W.; Roberts, E. P. L. Controlled Deposition of Nanoparticles at the Liquid–Liquid Interface. *Chem. Commun.* **2002**, 2324-2325.

[44] Platt, M.; Dryfe, R. A. W.; Roberts, E. P. L. Electrodeposition of Palladium Nanoparticles at the Liquid–Liquid Interface Using Porous Alumina Templates. *Electrochim. Acta* **2003**, *48*, 3037-3046.

[45] Chang, S. Y.; Booth, S. G.; Uehara, A.; Mosselmans, J. F. W.; Cibin, G.; Pham, V. T.; Nataf, L.; Dryfe, R. A. W.; Schroeder, S. L. M. Energy Dispersive-EXAFS of Pd Nucleation at a Liquid/Liquid Interface. *J.*

Phys.:Conf. Ser. **2016**, *712*, 012058.

[46] Booth, S. G.; Chang, S.-Y.; Uehara, A.; La Fontaine, C.; Cibin, G.; Schroeder, S. L. M.; Dryfe, R. A. W. In situ XAFS Study of Palladium Electrodeposition at the Liquid/Liquid Interface. *Electrochim. Acta* **2017**, *235*, 251-261.

[47] Yao, K.; Lu, W.; Li, X.; Wang, J. Tailoring the Properties of Aqueous–Ionic Liquid Interfaces for Tunable Synthesis and Self-Assembly of ZnS Nanoparticles. *J. Mater. Chem. A* **2014**, *2*, 5140–5148.

[48] Lu, W.; Yao, K.; Wang, J.; Yuan, J. Ionic Liquids-Water Interfacial Preparation of Triangular Ag Nanoplates and Their Shape-Dependent Antibacterial Activity. *J Colloid Interface Sci.* **2015**, *437*, 35-41.

[49] Soejima, T.; Kimizuka, N. Ultrathin Gold Nanosheets Formed by Photoreduction at the Ionic Liquid/Water Interface. *Chem. Lett.* **2005**, *34*, 1234-1235.

[50] Yao, K.; Huang, Q.; Lu, W.; Xu, A.; Li, X.; Zhang, H.; Wang, J. A Facile Synthesis of Gold Micro/Nanostructures at the Interface of 1,3-Dibutylimidazolium Bis(trifluoromethylsulfonyl)imide and Water. *J Colloid Interface Sci.* **2016**, *480*, 30-38.

[51] Yao, K.; Lu, W.; Li, X.; Wang, J.; Yuan, J. Tunable Synthesis of Ag Films at Ionic Liquid-Aqueous Interfaces. *Chem. Commun.* **2013**, *49*, 1398-1400.

[52] Chen, Y.; Chen, M.; Shi, J.; Yang, J.; Zhang, D. Fabrication of “Clean”

Nano-Structured Metal Materials on Ionic Liquid/Water Interface. *Mater. Lett.* **2014**, *132*, 153-156.

[53] Nishi, N.; Kakinami, T.; Sakka, T. Dendritic Nanofibers of Gold Formed by the Electron Transfer at the Interface Between Water and a Highly Hydrophobic Ionic Liquid. *Chem. Commun.* **2015**, *51*, 13638-13641.

[54] Nishi, N.; Yajima, I.; Amano, K. I.; Sakka, T. Janus-Type Gold/Polythiophene Composites Formed via Redox Reaction at the Ionic Liquid|Water Interface. *Langmuir* **2018**, *34*, 2441-2447.

[55] Zhang, Y.; Nishi, N.; Amano, K.; Sakka, T. One-Dimensional Pt Nanofibers Formed by the Redox Reaction at the Ionic Liquid|Water Interface. *Electrochim. Acta* **2018**, *282*, 886-891.

[56] Langmaier, J.; Trojánek, A.; Samec, Z. Electron Transfer Across the Polarized Interface Between Water and a Hydrophobic Redox-Active Ionic Liquid. *Electrochem. Commun.* **2010,** *12*, 1333-1335.

[57] Langmaier, J.; Samec, Z. Thermodynamic Aspects of the Electron Transfer across the Interface Between Water and a Hydrophobic Redox-Active Ionic Liquid. *Electrochim. Acta* **2011**, *58*, 606-613.

[58] Scholz, F.; Hasse, U. Controlling the Morphology of Silver Deposition at Liquid|Liquid Interfaces: From Nano-Wires to Super Smooth Films. *Electrochem. Commun.* **2005**, *7*, 541-546.

[59] Shanthi, K.; Vimala, K.; Gopi, D.; Kannan, S. Fabrication of a PH

Responsive DOX Conjugated PEGylated Palladium Nanoparticle Mediated Drug Delivery System: An In Vitro and In Vivo Evaluation. *RSC Adv.* **2015**, *5*, 44998-45014.

[60] Kakiuchi，T.; Tsujioka，N.; Sueishi，K.; Nishi, N.; Yamamto, M. Polarized Potential Window Available at the Interface Between an Aqueous Electrolyte Solution and Tetraalkylammonium Imide Salts *Electrochemistry* **2004**, *12*, 833-835.

[61] Nishi, N.; Imakura, S.; Kakiuchi, T. A Digital Simulation Study of Steady-State Voltammograms for the Ion transfer Across the Liquid–Liquid Interface Formed at the Orifice of a Micropipette. *J. Electroanal. Chem.* **2008**, *621*, 297-303.

[62] Booth, S. G.; Dryfe, R. A. W. Assembly of Nanoscale Objects at the Liquid/Liquid Interface. The Journal of Physical Chemistry C **2010**, *119*, 23295-23309.

[63] Kim, K.; Han, H. S.; Choi, I.; Lee, C.; Hong, S.; Suh, S. H.; Lee, L. P.; Kang, T. Interfacial liquid-state surface-enhanced Raman spectroscopy. *Nat. Commun.* **2013**, *4*, 2182.

[64] Velleman, L.; Scarabelli, L.; Sikdar, D.; Kornyshev, A. A.; Liz-Marzan, L. M.; Edel, J. B. Monitoring plasmon coupling and SERS enhancement through in situ nanoparticle spacing modulation. *Faraday Discuss.* **2017**, *205*, 67-83.

[65] Zhao, Y.; Zhan, L.; Tian, J.; Nie, S.; Ning, Z., Enhanced Electrocatalytic Oxidation of Methanol on Pd/Polypyrrole–Graphene in Alkaline Medium. *Electrochim. Acta* **2011**, *56*, 1967-1972.

[66] Singh, R. N.; Singh, A.; Anindita, Electrocatalytic Activity of Binary and Ternary Composite Films of Pd, MWCNT and Ni, Part II: Methanol Electrooxidation in 1M KOH. *Int. J. Hydrogen Energ.* **2009**, *34*, 2052-2057.

Figures

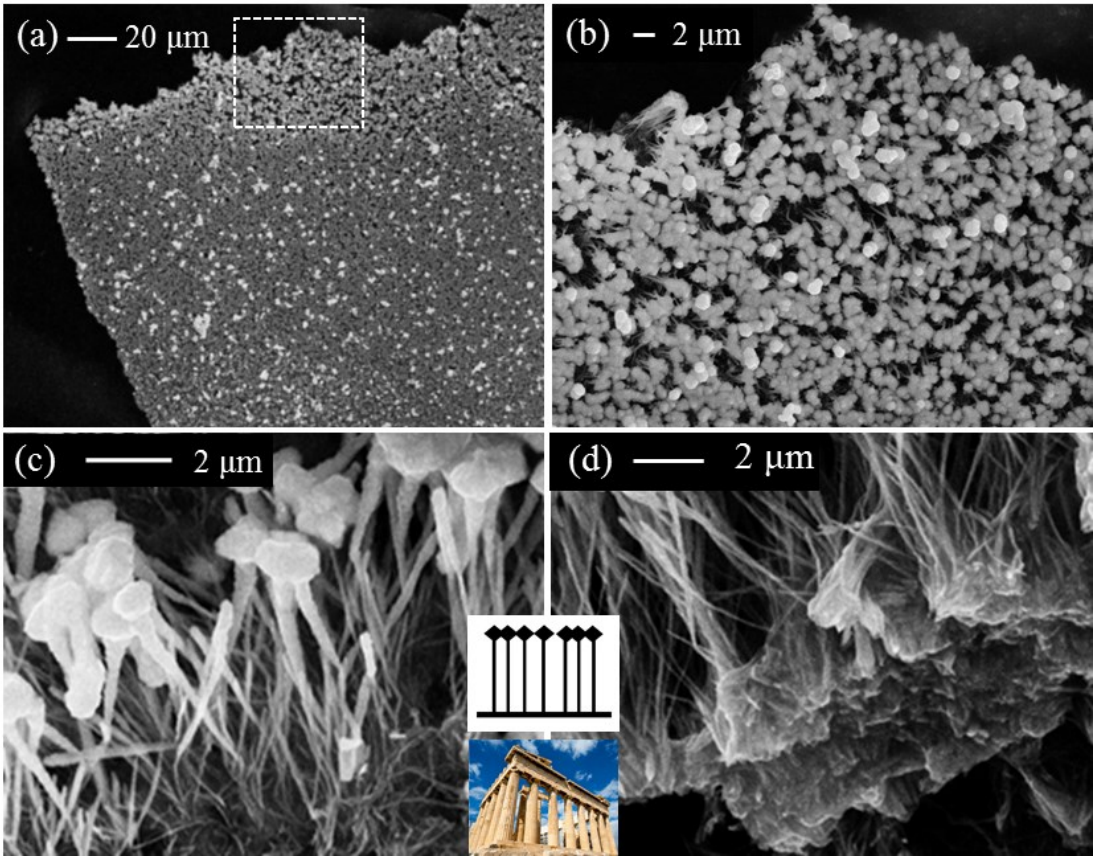

Figure 1. SEM images of the Pd NFAs for the reaction time t = 20 h with (a) a low resolution and (b) a high resolution for the marked region in (a); (c and d) the lateral profiles; Insets: structure schematic of the Pd NFAs and an analogous architectural design in reality.

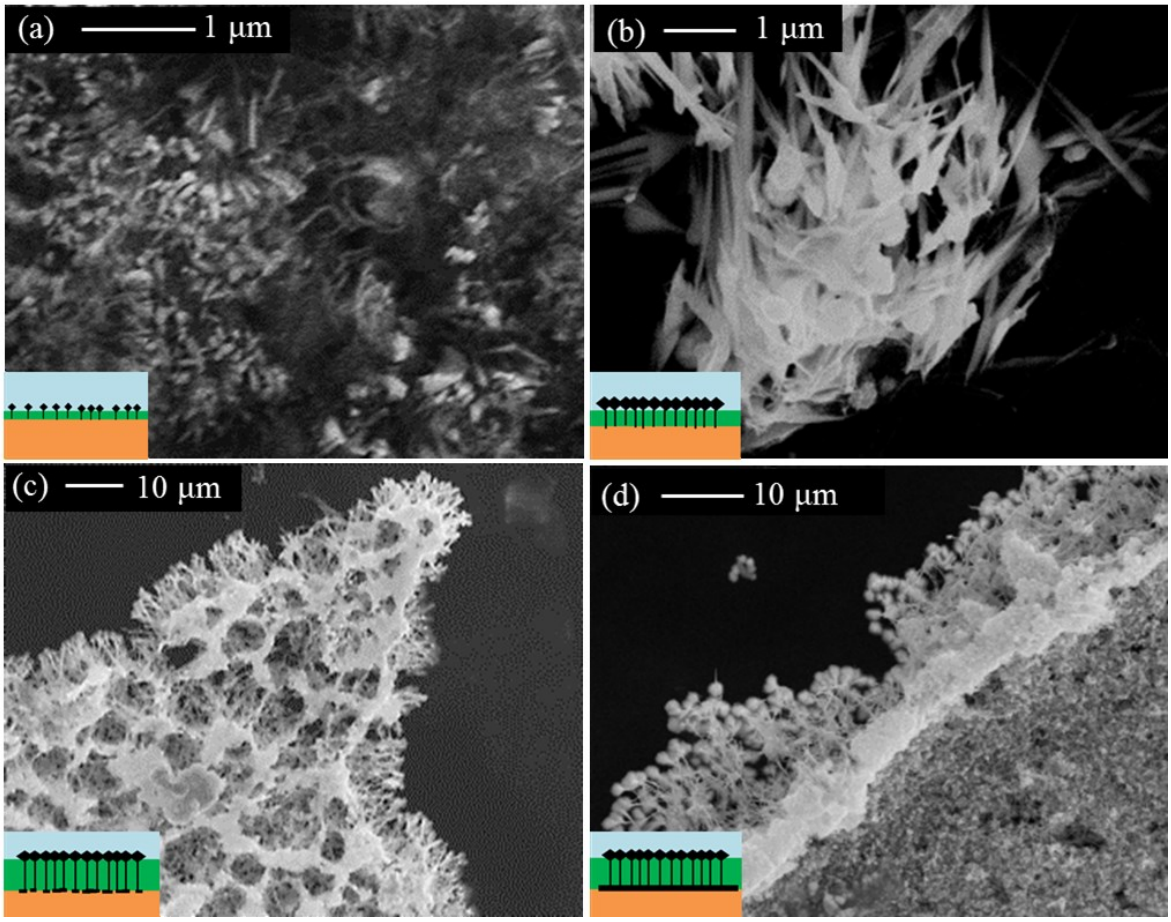

Figure 2. Time dependence of the morphology of the Pd NFAs for t = (a) 1, (b) 4, (c) 12, and (d) 20 h. The other conditions are the same as the standard synthesis process. For the nanostructures in (a) and (b), the original orientations are not preserved, and hence, they are randomly oriented but those in (c) and (d) are viewed from the bottom.

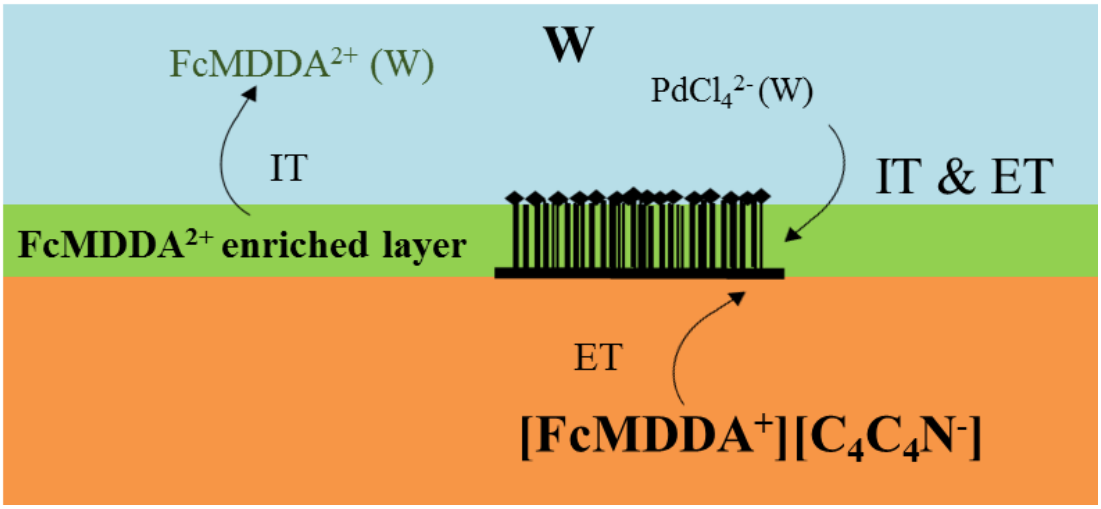

Figure 3. Schematic for a possible mechanism of the spontaneous formation of Pd NFAs.

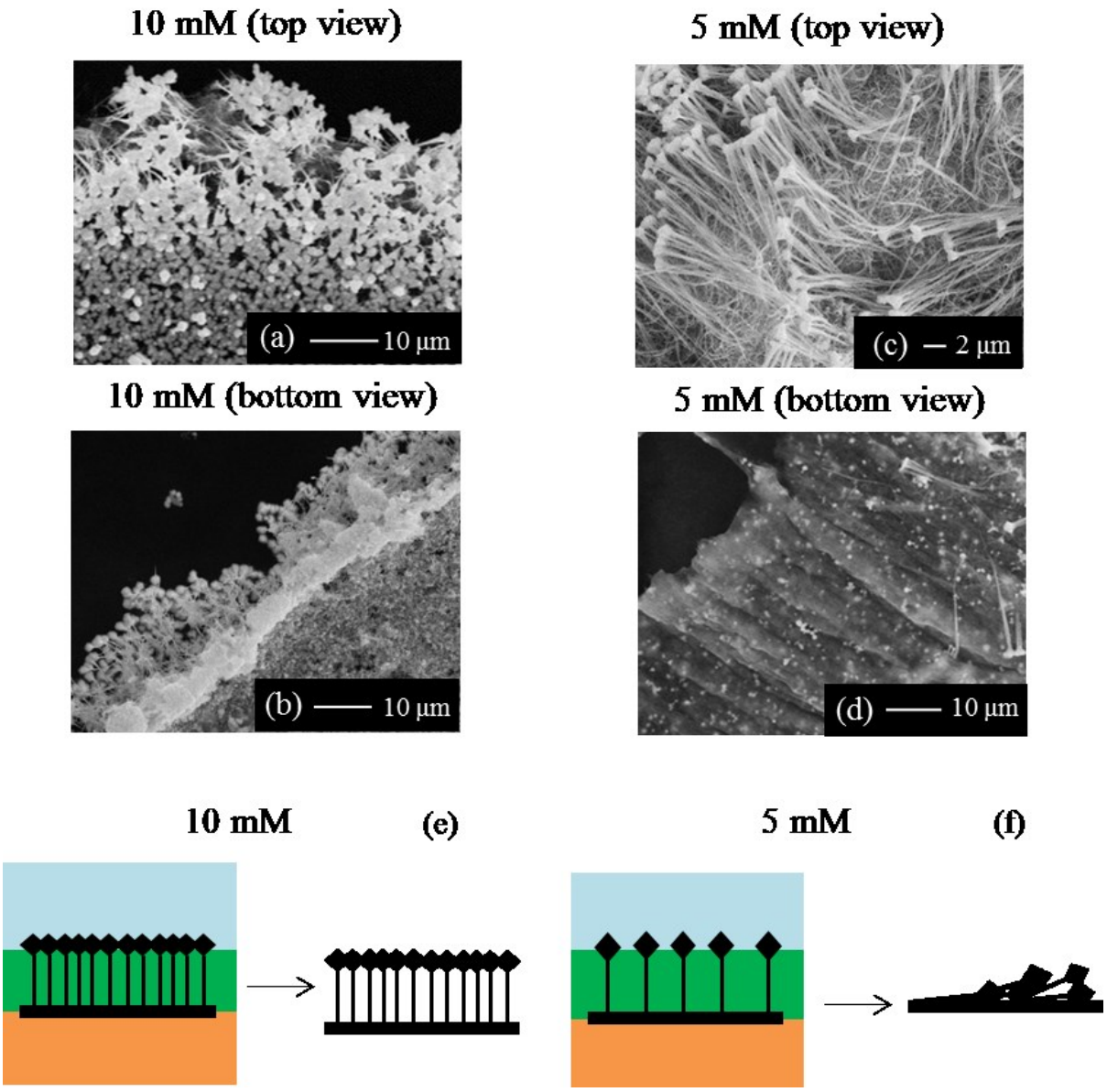

Figure 4. SEM images of top side (a, c) and bottom side (b, d) of (a, b) the Pd NFAs obtained with a typical synthesis condition, (c, d) the Pd nanostructures obtained with the concentration of $PdCl_4^{2-}$ in W decreased from 10 mM to 5 mM. (e, f) Schematics of the formation mechanism of Pd NFAs.

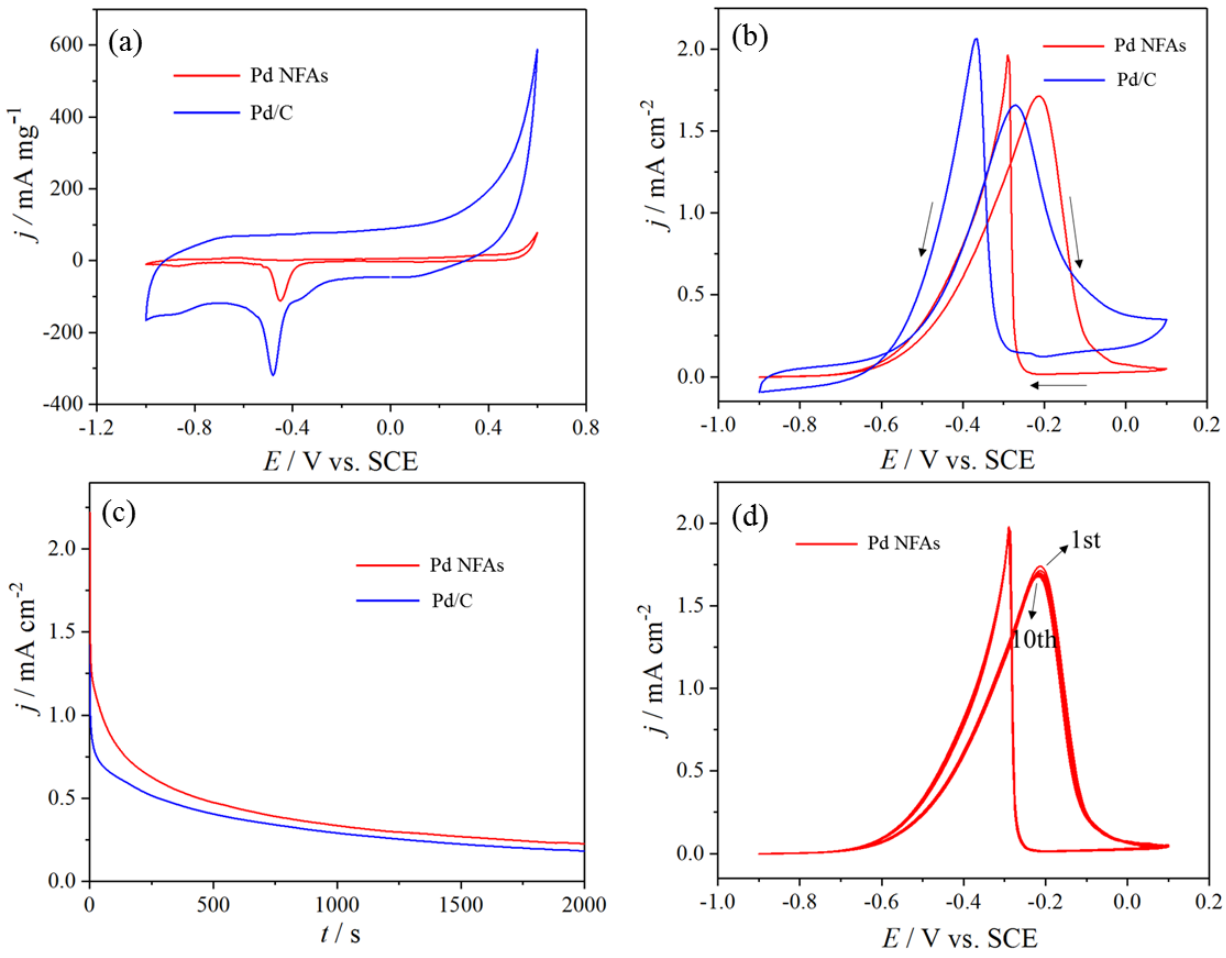

Figure 5 (a) CVs of Pd NFAs and Pd/C in a 1 M NaOH solution at 50 mV/s and then normalized by the loading amount of Pd (5.0 μg for Pd NFAs and 1.0 μg for Pd/C); (b) CVs of Pd NFAs and Pd/C in a 1 M NaOH + 1 M ethanol solution at 50 mV/s and then normalized by the EASA of Pd; (c) CAs of Pd NFAs and Pd/C in a 1 M NaOH + 1 M ethanol solution at an applied voltage of –0.3 V for 2000 s and then normalized by the EASA of Pd; (d) CV of Pd NFAs in a 1 M NaOH + 1 M ethanol solution at 50 mV/s for 10-time cycles.

For Table of Contents Only